nature communications

Article

https://doi.org/10.1038/s41467-026-74082-0

The *Bacillus subtilis* circadian clock coordinates intricate spatiotemporal organisation

Received: 12 March 2026

Accepted: 22 May 2026

Published online: 18 June 2026

Check for updates

Jack Dorling[1,8], Francesca Sartor[2,8], Borja Ferrero-Bordera[2], Edward Godfrey[2,5], Zheng Eelderink-Chen[2,6], Ella Baker[1], Isobel K. Banks[1], Akshat Joshipura[2,7], Xinming Xu[3], Romain Avellan[3], Ákos T. Kovács[3], Antony N. Dodd[1] ✉ & Martha Merrow[2,4] ✉

Many organisms have circadian clocks that anticipate the risks and benefits of the predictable 24 h solar cycle. However, the potential functions of circadian clocks in non-photosynthetic bacteria are poorly understood. Here, we show that the *Bacillus subtilis* circadian clock regulates colony expansion, in concert with key developmental and differentiation pathways that are central to its life cycle. The *B. subtilis* clock coordinates the spatiotemporal organisation of gene expression within expanding colonies by timing various processes to specific phases (times of day) within distinct colony regions. Our results support the idea that circadian clock-regulation over space, time and colony development in *B. subtilis* is analogous to circadian regulation of some processes in multicellular eukaryotes such as plants and mammals.

Circadian clocks time daily rhythms in organelles, cells, organs, organisms and organismal interactions[1]. They control diverse gene and protein expression, alongside physiological, metabolic, and behavioural processes, orchestrating daily temporal programs across scales[2]. Endogenous circadian clocks produce free-running, *circa* 24 h rhythms in constant conditions, which synchronize (entrain) to environmental cues called zeitgebers (time-givers). In doing so, they contribute to fitness by allowing time-of-day-specific anticipation of both stressful and favourable environmental conditions[3].

Until recently, detailed knowledge of prokaryotic circadian rhythms was restricted to photosynthetic cyanobacteria[4] and the human gut bacterium *Klebsiella aerogenes*[5]. We discovered a circadian clock in biofilm-forming cultures of the non-photosynthetic bacterium *Bacillus subtilis*[6]. Biofilm formation is of ecological and medical importance, and is characterized by cellular aggregation, matrix production, and, in *B. subtilis*, spore formation[7]. Given that *B. subtilis* possesses a circadian clock and exhibits spatiotemporal patterning of cell differentiation[8–11], we investigated the hypothesis that its circadian clock functions as an organizer of growth and differentiation. Our data demonstrate that the *B. subtilis* clock acts as a master regulator that orchestrates the spatiotemporal organization of colony expansion and cell differentiation pathways over each daily cycle. Therefore, we advance previous observations of circadian clock regulation of gene expression and identify here that the clock regulates colony morphology and development, thus establishing functional consequences of the *B. subtilis* circadian clock.

Results

B. subtilis exhibits circadian clock-regulated concentric ring formation on soft agar

Striking concentric patterns of colony expansion occur in several bacterial species[12]. Soft agar media was inoculated with *B. subtilis*

[1]Department of Cell and Developmental Biology, John Innes Centre, Norwich Research Park, Norwich, UK. [2]Institute of Medical Psychology, Faculty of Medicine, University of Munich, Munich, Germany. [3]Institute of Biology, Leiden University, Leiden, Netherlands. [4]Radcliffe Department of Medicine, University of Oxford, Oxford, UK. [5]Present address: School of Engineering Mathematics and Technology, University of Bristol, Bristol, UK. [6]Present address: Department for Molecular Toxicology, Helmholtz Centre for Environmental Research GmbH – UFZ, Leipzig, Germany. [7]Present address: Institute for Molecular Immunology, Technical University of Munich, Munich, Germany. [8]These authors contributed equally: Jack Dorling, Francesca Sartor.
✉e-mail: antony.dodd@jic.ac.uk; martha.merrow@med.uni-muenchen.de

https://doi.org/10.1038/s41467-026-74082-0

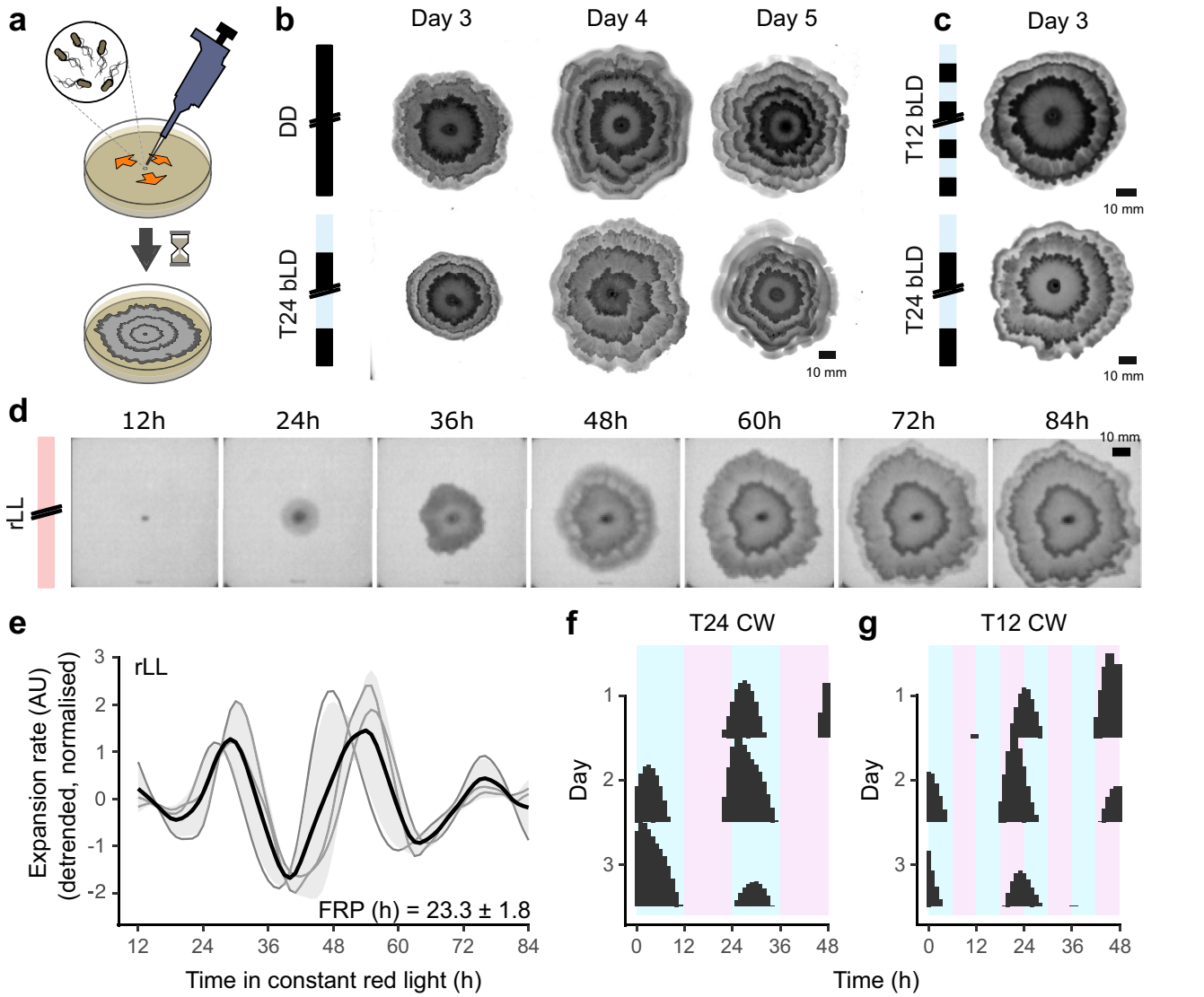

Fig. 1 | The circadian clock regulates the expansion rate and spatial patterning of *B. subtilis* colonies. a *B. subtilis* 168 Jena was spotted onto semi-solid LB agar and allowed to expand across the agar surface for 3-5 days. **b** End-point images of colonies from 3 to 5 days incubation in DD or T24 bLD (30 µmol m^{-2} s^{-1}). **c** Images of colonies formed under either T12 bLD or T24 bLD (30 µmol m^{-2} s^{-1}). **d** Time-series imaging under rLL (13 µmol m^{-2} s^{-1}). Scale bar represents 10 mm. See Supplementary Movie S1 for time-lapse of images in **d**. **e** Circadian rhythm of expansion rate of colonies growing in rLL (13 µmol m^{-2} s^{-1}; $n = 3$) using colony area data from time-series imaging (as in **d**). Free running periods were determined by FFT-NLLS, for data between 12 to 84 h. See Supplementary Data 1 for rhythmicity statistics. Black line, mean; grey areas, standard deviation (SD). **f** Double plot of colony expansion rate under T24 CW temperature cycles and (**g**) T12 CW temperature cycles in rLL (13 µmol m^{-2} s^{-1}; temperatures: 25.5 °C and 28.5 °C). Pink and light blue indicate warm and cold, respectively; black areas indicate expansion rates greater than the daily mean. AU = arbitrary units. See Supplementary Fig. 4 for biological replicates.

strain 168 Jena (hereafter called 168; Fig. 1a) and incubated for 3 to 5 days in free-running or entraining conditions (constant darkness (DD) or 24 h zeitgeber cycles of 12 h blue light and 12 h darkness (T24 bLD), respectively; Fig. 1b and Supplementary Fig. 1a). Blue light (e.g., T24 bLD) is a zeitgeber used by the *B. subtilis* clock for entrainment[6]. Concentric rings formed with a frequency of about one per day under both conditions, an interval consistent with endogenous circadian timing. In other model circadian clock systems, an oscillator with a period of about 24 h directs a rich landscape of clock-controlled processes (outputs)[13,14]. We examined whether these basic properties of circadian clocks – entrainment using zeitgebers, endogenous *circa*-24 h rhythm generation, and clock-regulated outputs – were represented in the ring-forming *B. subtilis* colonies.

Light is the single most pervasive zeitgeber that circadian systems use for entrainment[15]. We previously demonstrated that circadian rhythms of reporter gene expression in *B. subtilis* entrain under 24 h blue and/or red-light cycles[6,16]. We thus compared ring formation in DD, constant red or constant blue light (rLL or bLL, respectively), T24 bLD, and 24 h cycles of red light and darkness (12 h rL/12 h D, T24 rLD; Supplementary Fig. 1a). One ring formed per day under all tested conditions, consistent with regulation by a circadian clock. Circadian clock regulation was confirmed by testing for frequency demultiplication. This is a powerful tool, whereby a biological oscillator synchronizes to environmental cycles outside the range of entrainment[17] if the frequency is a submultiple of its own[18]. For instance, using a 12 h cycle, a harmonic of 24 h, leads to entrainment to each second cycle[18,19]. Thus, we used bLD cycles lasting 12 h per cycle rather than 24 h (T12 bLD; 6 h bL and 6 h D). In T12 bLD, a single ring formed each 24 h (Fig. 1c), demonstrating an underlying, robust,

entraining, circadian system. Therefore, ring formation on soft agar is circadian clock-regulated.

Ring formation was differentially modulated by the spectral quality of light. Under illumination with blue light (bLL and T24 bLD), approximately one ring per day continued to form (Supplementary Fig. 1a) but overall colony expansion was reduced compared with DD (Supplementary Fig. 1b). No differences in colony area occurred after culture in either rLL or T24 rLD cycles relative to DD (Supplementary Fig. 1b). Growth of 168 in liquid LB medium confirmed that constant blue light leads to delayed growth compared with cultures grown in DD or rLL (Supplementary Fig. 1c). Thus, light is a zeitgeber for the *B. subtilis* clock and its spectral quality effects colony expansion.

Analysis of time-series photography in dim rLL (Fig. 1d, Supplementary Movie 1) revealed a striking, high amplitude, 4-fold daily oscillation in the rate of colony expansion each 24 h (Fig. 1e; mean Free Running Period (FRP) = 23.3 ± 1.8 h). In another *B. subtilis* strain (JH642; derived from 168[20–22]), the FRP of colony expansion rate was 21.0 ± 0.79 h, with a similar amplitude (Supplementary Fig. 2a, b; Supplementary Movie 2). Cell number was evaluated at different locations within mature colonies (Supplementary Fig. 3a, b; inner versus edge ring regions). There were no differences in cell number (Supplementary Fig. 3a, b), showing that expansion rate rhythms do not create lasting variations in cell density across the mature colony.

In addition to light, temperature is a common zeitgeber for circadian clocks because it changes predictably over daily LD cycles. We previously demonstrated entrainment of the *B. subtilis* clock to T24 temperature cycles[6]. Colony expansion rate was compared in T24 (Fig. 1f, Supplementary Fig. 4a) and T12 (Fig. 1g, Supplementary Fig. 4b) warm/cool (CW) cycles (rLL, 25.5 °C/28.5 °C), showing that colony expansion rate peaked once per day in both conditions, again demonstrating frequency demultiplication. Therefore, colony expansion rate within this assay is controlled by a circadian clock.

Many bacteria exhibit collective behaviour in appropriate conditions, which is an adaptive strategy important for their ecology[23,24]. How does *B. subtilis* colony ring formation compare with rings formed by other bacteria? Daily colony ring formation in the gut bacterium *Klebsiella aerogenes* results from rhythmic swarming[5]. *B. subtilis* strain 168 cannot swarm due to a mutation in the gene *swrA*[25,26]. An additional swarming-defective strain, JH642, also produced concentric rings when cultured on soft agar (DD, 27 °C, 3 days; Supplementary Fig. 2a, b). We tested ring formation in the swarming-proficient *B. subtilis* strains PS216, MB9_B1, MB8_B1, and NCIB 3610. These strains rapidly and uniformly colonized the entire agar surface, whereas swarming-deficient 168 expanded slowly and produced a ring pattern (Supplementary Fig. 5a, b). We also investigated whether biofilm matrix production was necessary for colony expansion[27–29] and concentric ring pattern formation, by examining growth on soft agar of two mutants lacking specific matrix components (Δ*epsA-O* and Δ*tasA* deficient in exopolysaccharide and protein fibre production, respectively), and also several weak biofilm-forming strains (Supplementary Fig. 5c). These strains did not spread across the soft agar or form visible rings, whereas in liquid culture the strains grew similarly to the 168 Jena strain (Supplementary Fig. 5d).

In both *Pseudomonas aeruginosa* and *Listeria monocytogenes*, concentric rings form on soft agar[30,31] but this occurs only under 24 h LD cycles, and not in constant conditions as for *B. subtilis* (e.g. Figures 1b, 1d; Supplementary Fig. 1a). The observations described for *P. aeruginosa* and *L. monocytogenes* are characteristic of driven rather than circadian phenotypes, as confirmed in *P. aeruginosa*[31]. The ring pattern in *L. monocytogenes* requires the blue light photoreceptor Lmo0799, which is a homologue of *B. subtilis* YtvA[6,16]. YtvA has a clock-regulated promoter[6]. In *B. subtilis*, *ytvA* deletion does not affect ring formation under DD, indicating that YtvA is not an essential part of the circadian clock mechanism that is necessary to produce this ring pattern (Supplementary Fig. 6a). Blue light suppression of colony expansion occurred through a blue light response pathway independent of YtvA (Supplementary Fig. 6b). Therefore, despite phenotypic similarities, concentric ring formation in *B. subtilis* arises from a mechanism that is distinct from those in *K. aerogenes*[5], *P. aeruginosa*[31], and *L. monocytogenes*[30].

Clock regulation of gene expression in expanding colonies

We previously demonstrated circadian clock-regulated expression of a reporter gene (P_{ytvA}-*luxABCDE* (P_{ytvA}-*lux*)) in pellicle-forming biofilm cultures of *B. subtilis* 168[6]. Therefore, we used this gene as a reporter for the circadian clock in expanding colonies. Imaging of P_{ytvA}-*lux* bioluminescence over 5 days of DD revealed remarkable rhythmic patterns of P_{ytvA}-*lux* bioluminescence as colonies expanded (Fig. 2a; Supplementary Movie 3). The rhythms in whole-colony bioluminescence (Fig. 2b) and bioluminescence at the growing colony edge (Fig. 2c), where bioluminescence appeared to consolidate (Supplementary Movie 3), had circa-24 h free-running periods. As in T24 bLD, T12 bLD cycles yielded a single P_{ytvA}-*lux* bioluminescence peak that occurred each 24 h at the growing colony edge, again demonstrating frequency demultiplication (Fig. 2d; Supplementary Fig. S7a, and S7b; Supplementary Movies 4, 5). Therefore, expression from the *ytvA* promoter in expanding colonies is regulated by the circadian clock, as in pellicle biofilm-forming liquid cultures[6].

A separate ring-formation phenotype that has shorter periods, of 4-16 hours, has been reported for biofilm colonies of *B. subtilis*[9,32]. Generation of this spatiotemporal patterning involves electrochemical communication within the expanding colony and depends on the potassium channel YugO. Therefore, we tested how such ultradian oscillations might relate to the circadian clock-regulated ring phenotype that we observed. We compared the circadian rhythms of colony expansion and P_{ytvA}-*lux* bioluminescence in the wild-type and a *yugO* deletion strain (P_{ytvA}-*lux* Δ*yugO*) (Supplementary Fig. 8). The oscillations of colony expansion rate and P_{ytvA}-*lux* bioluminescence were unaltered in Δ*yugO* compared to the wild type (Supplementary Fig. 8a–e). This suggests that the clock-regulated ring patterns that we observed do not depend on potassium channels that drive the previously described ultradian oscillations in biofilm colonies.

B. subtilis cell differentiation pathways are circadian clock-controlled

Cell differentiation occurs extensively in *B. subtilis* biofilm and is a crucial part of its life history, ecology, and fitness[7]. We hypothesized that colony ring formation involves clock regulation of these differentiation processes. Two key differentiation processes are biofilm production and sporulation. The former involves a transition from a motile, planktonic cell state to a sessile, collective cell state in which emergent properties manifest[7]. The latter involves development into metabolically inactive cells, called spores, whose production allows survival of adverse environmental conditions. Therefore, we examined the temporal regulation of genes and operons associated with biofilm matrix production (*epsA-O* and *tapA-sipW-tasA*) and sporulation (early: *spoIIG-sigE-sigG*, mid: *spoIIQ*, late: *spoIID*) in a pellicle assay (Fig. 3a) that supports circadian rhythm detection[6,16]. After entrainment of the cultures to bLD cycles, promoter-driven luciferase reporters had self-sustained oscillations in the circadian range in DD, similar to P_{ytvA}-*lux* (Fig. 3b; Supplementary Fig. S9a, S9b). This suggests clock control of pathways that regulate biofilm matrix production and sporulation.

Given that the clock controls differentiation pathway gene expression in pellicle biofilms and concentric ring development in expanding colonies, we investigated the spatiotemporal regulation of luciferase reporter gene expression for these differentiation pathways in expanding colonies. In DD, there were *circa* 24 h rhythms in the activity of promoters involved in biofilm (*epsA*, *tapA*) and sporulation (*spoIIG*, *spoIID*) at both the growing colony edge and concentric inner regions of the colony (Figs. 3c–g, Supplementary Movies 6-9). The

https://doi.org/10.1038/s41467-026-74082-0

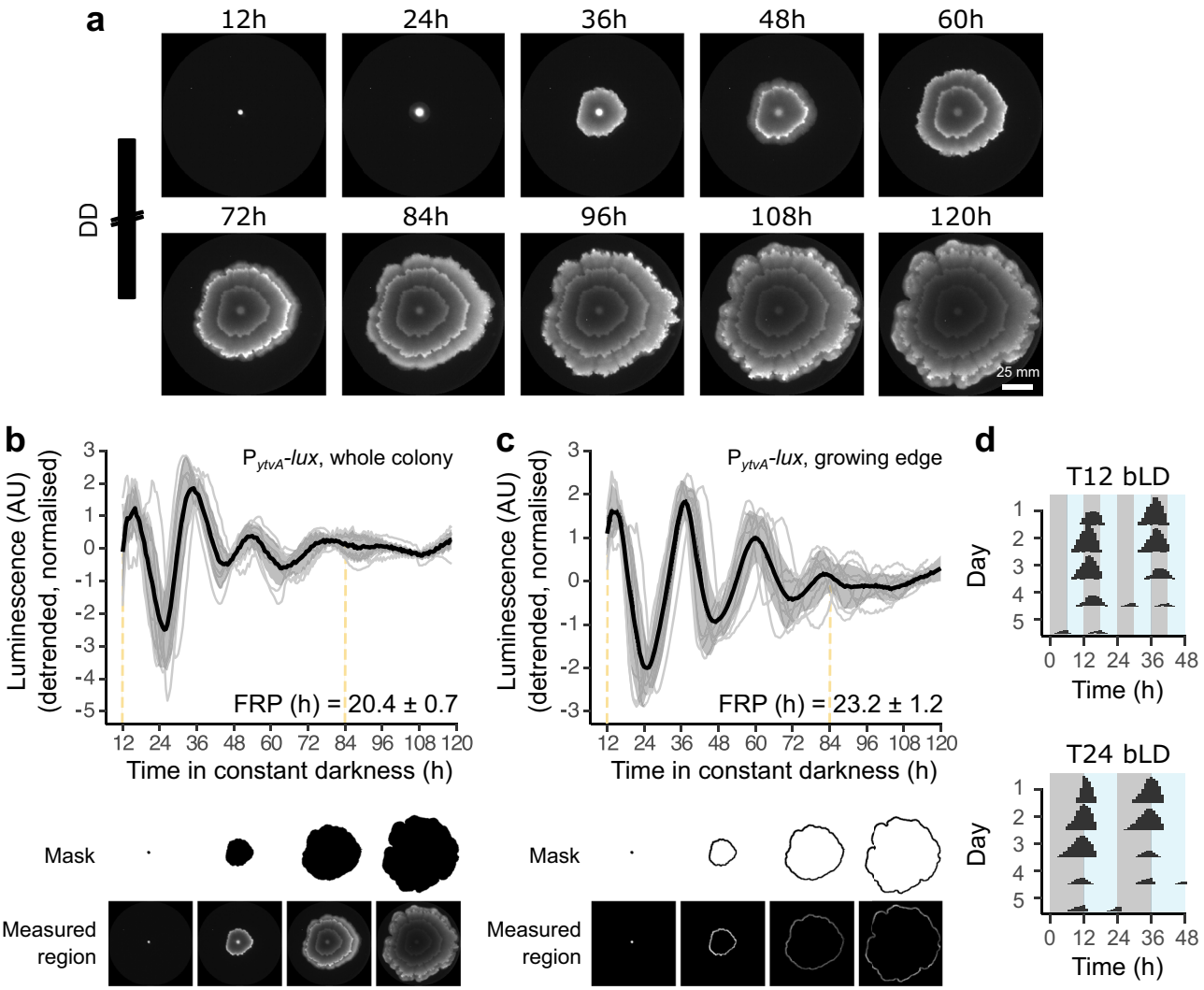

Fig. 2 | Robust circadian rhythms in *ytvA* promoter activity in whole colony and growing colony edge. a P$_{ytvA}$-*lux* bioluminescence in *B. subtilis* 168 during colony expansion in DD (Supplementary Movie 2). Scale bar, 25 mm. **b** Bioluminescence of the entire colony. **c** Bioluminescence at the colony edge, as it expanded. Black lines, mean; thin grey lines, individual replicates; grey areas, SD ($n = 9$). The diagrams below respective graphs of masked regions of images that are measured (see below) and plotted (see above). FRPs were determined by FFT-NLLS for data between 12 and 84 h (vertical dashed lines). See Supplementary Data 1 for rhythmicity statistics. **d** Double plots showing P$_{ytvA}$-*lux* bioluminescence from the growing colony edge under T12 bLD (upper) or T24 bLD (lower) cycles (30 µmol m^{-2} s^{-1}). See also Supplementary Fig. 7 and Supplementary Movies 3 and 4 for time-lapses of colonies imaged under T12 bLD and T24 bLD, respectively. AU arbitrary units. Blue and grey areas represent light and dark periods, respectively.

colony expansion rate FRP was ~24 h for all reporter strains (Supplementary Fig. 10a–f). Intriguingly, the FRP of the bioluminescence rhythm at the growing colony edges correlated significantly with the FRP of the colony expansion rate (Fig. 3h, Supplementary Fig. 11a). As a functional readout of biofilm formation, we challenged biopsies of inner (opaque) and edge (translucent) colony regions with bactericidal levels of H_2O_2, because biofilm is known to protect against oxidative stress[30,33]. A significantly greater proportion of cells from the edge regions of the rings survived this treatment (Fig. 3i). Thus, promoter activity is reflected in functional aspects of biofilm matrix production. This suggests control of multiple, distinct developmental processes in *B. subtilis* by its circadian clock.

Spatiotemporal organization within expanding colonies by the *B. subtilis* clock

Circadian clocks are cell-based[34]. When a population is formed from different, interacting cell types, this poses an organizational challenge. Individual cellular rhythms must be appropriately synchronised and coordinated within the population, which is essential to yield a cohesive, emergent circadian system. This principle is known as circadian organization.

The spatiotemporal patterns of gene expression in expanding colonies presented a unique opportunity to document circadian behaviour in both time and space, providing insights into circadian organization of a simple yet informative system. Each rhythmic promoter yielded distinct spatiotemporal activity patterns of gene expression relative to expansion rate. These clock-regulated phenotypes had differing positions – corresponding to distinct internal phase relationships - within the dynamically expanding colony (DD conditions; Fig. 3c–f; Supplementary Movies 3, 6–9). P$_{epsA}$-*lux* and P$_{tapA}$-*lux* were expressed at the growing edge, P$_{ytvA}$-*lux* was expressed behind the growing edge, and P$_{spoIIG}$-*lux* and P$_{spoIID}$-*lux* were expressed further behind P$_{ytvA}$-*lux* (Supplementary Movies 3, 6–9). Expression of P$_{ytvA}$-*lux* gradually faded in the inner colony areas, whereas P$_{tapA}$-*lux* became inactive (Fig. 3d). P$_{epsA}$-*lux* and P$_{spoIID}$-*lux* reinitiated expression at the formed rings of the colonies after 2 days (Figs. 3c, f) whereas P$_{spoIIG}$-*lux* had similar but reduced bioluminescence at the ring edges (Fig. 3e). These observations demonstrate promoter-specific

https://doi.org/10.1038/s41467-026-74082-0

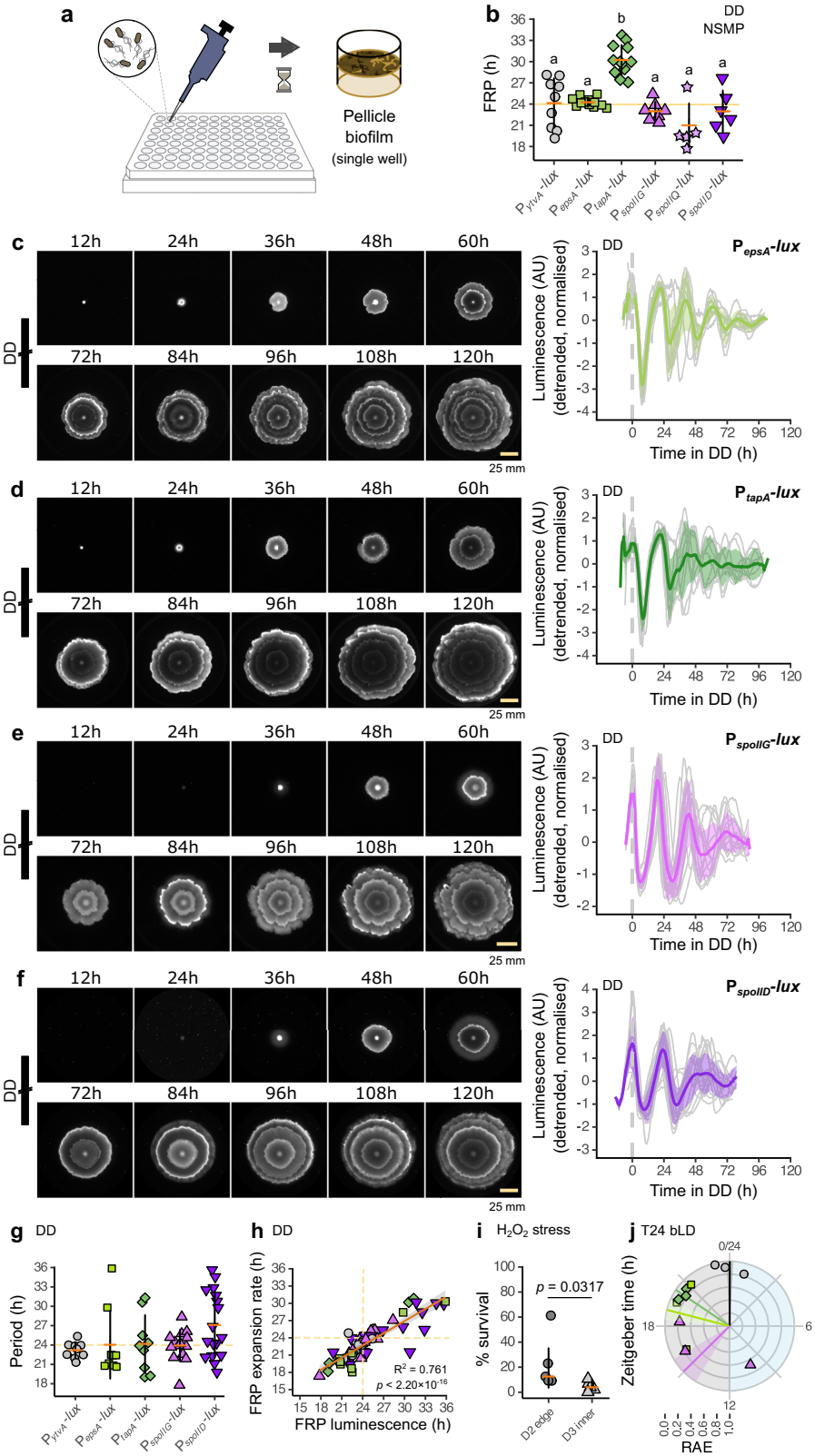

regulation of these reporters by the clock and predict unique entrainment properties of their expression in zeitgeber cycles[35], which is a key feature of circadian clocks. In T24 bLD, rhythms of different reporter genes assumed different phases (entraining to different times of day; Fig. 3j, and S12a – 11c; and in Supplementary Movies 5, 10–12). This variety of phases is reminiscent of relative phase relationships between rhythms in different organs of mice[36].

We analysed circadian organization in these colonies in more detail. Colony images were digitally linearized and the bioluminescence signal of individual radial colony sections from all timepoints was stacked side-by-side to create kymographs (Fig. 4a; see Supplementary Fig. S13a–e for average intensity projections across all radial sections). This visualizes the spatial distribution of promoter activity within the expanding colony over time in a single image. The 24 h

https://doi.org/10.1038/s41467-026-74082-0

Fig. 3 | The *B. subtilis* circadian clock regulates differentiation pathways similarly to expansion rate. (**a**) Pellicle biofilm cultures were incubated in 96-well plates. **b** Bacteria were released to DD for 3 d after 5 d in 24 h bLD cycles. FRPs of P_{ytvA}-*lux*, P_{epsA}-*lux*, P_{tapA}-*lux*, P_{spoIIG}-*lux*, P_{spoIIQ}-*lux*, and P_{spoIID}-*lux*, all in the 168 background, are reported (One-way ANOVA: $F_{5,47} = 18.01$, $p < 0.0001$). P_{tapA}-*lux* was significantly different from all other reporters ($p < 0.0001$, Tukey´s multiple comparison test, samples marked with 'a' are not significantly different from one another; $p >= 0.05$). Means and SDs are indicated. See Supplementary Fig. 9 for bioluminescence time-series. Bioluminescence imaging of expanding colonies of 168 P_{epsA}-*lux* (**c**), P_{tapA}-*lux* (**d**), P_{spoIIG}-*lux* (**e**) and P_{spoIID}-*lux* (**f**) in DD (Supplementary Movies 5-8; see Supplementary Data 1 for additional information) and resulting circadian rhythms in colony growing edge bioluminescence. Scale bars, 25 mm. Coloured lines, mean; corresponding shaded areas show SD. All colonies were rhythmic for growing edge bioluminescence (all reporters: $p_{BH_corr} \leq 1.00 \times 10^{-5}$; Supplementary Data 1) with FRPs reported in (**g**) (One-way ANOVA: $F_{4,53} = 1.97$, $p = 0.113$). Data for P_{ytvA}-*lux* are carried over from Fig. 2c. Means and SD are shown. **h** Correlation between FRP of growing edge bioluminescence (all reporters) and colony expansion rate in DD (see R^2 and p values. Linear model fit, line; grey area, 95% confidence intervals. Within the linear model, the residual standard error is 1.668 on 56 degrees of freedom; F = 183.2. See also Supplementary Fig. 10, 11. (**i**) Survival of bacterial cells sampled from the edge and inner regions of colony rings formed on day 2 and day 3, respectively, after hydrogen peroxide exposure ($n = 5$, $p = 0.0317$, two-tailed Mann-Whitney test). Median and inter-quartile range is shown. **j** Phase of peak edge bioluminescence rhythms for P_{ytvA}-*lux*, P_{epsA}-*lux*, P_{tapA}-*lux* and P_{spoIIG}-*lux* ($n = 3$) in T24 bLD (30 µmol m^{-2} s^{-1}). Phase is expressed relative to dawn (ZT0), normalised for FRP and furthermore plotted as relative amplitude error (RAE). See Supplementary Movies 9-11 (T24 bLD) and Supplementary Fig. 12 for corresponding bioluminescence data, colony expansion rate data and the corresponding colony expansion rate phase. AU arbitrary units. Circular means for phase (coloured lines) and standard deviation (coloured shading) are shown with symbols and colours as in (**g**). Different coloured data traces indicate different luciferase reporter strains.

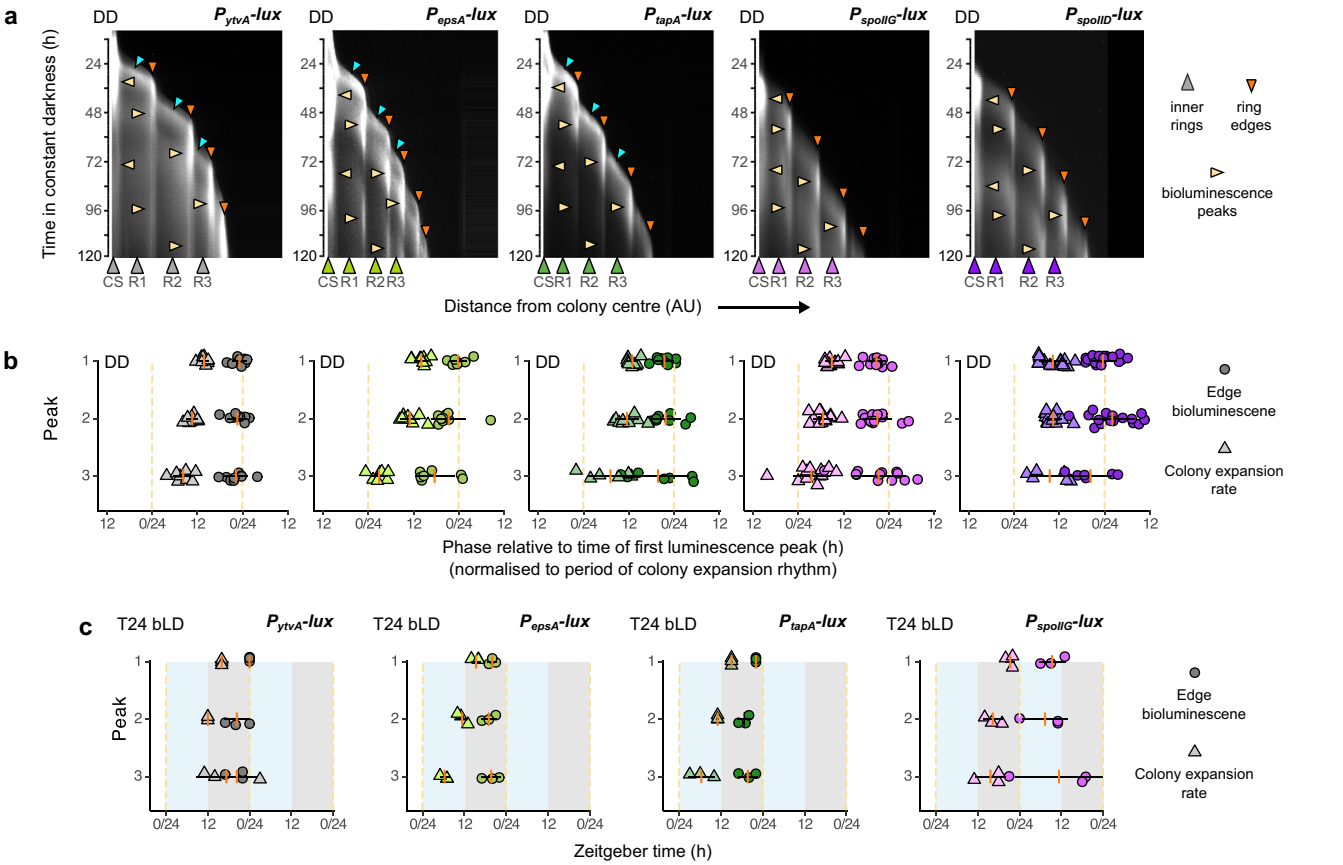

Fig. 4 | Spatiotemporal organization of circadian clock-regulated promoter activation in *B. subtilis*. **a** Example kymographs for all reporters, whereby the vertical axis represents time, the horizontal axis the radial distance from colony centre, and the grey scale the bioluminescence signal intensity. The central spot (CS; inoculation site) and resulting first (R1), second (R2) and third colony rings (R3) are marked on horizontal axes. Ring edges and inner rings are marked with orange and gray arrowheads, respectively. Bioluminescence peaks are marked with yellow arrowheads. See Supplementary Fig. 13a–e for kymographs of experimental replicates. **b** Peak times of rhythms of edge bioluminescence and colony expansion rate in constant darkness. Mean and SD are shown. **c** Peak times of edge bioluminescence and colony expansion rate in T24 bLD cycles (30 µmol m^{-2} s^{-1}). Light blue and grey shading denote light and dark periods, respectively. Error bars show SD. **b**, **c** Different coloured data points indicate different luciferase reporter strains. P_{ytvA}-*lux*, P_{epsA}-*lux*, P_{tapA}-*lux* $n = 9$; P_{spoIIG}-*lux* $n = 14$; P_{spoIID}-*lux* $n = 17$.

cycles of colony expansion and pausing, which explain the circadian rhythm in colony expansion rate, are clearly visible (Fig. 4a). For P_{ytvA}-*lux*, expression behind the colony growing edge is clearly visible (blue arrows) with greatest expression when colony expansion paused, persisting at the edge even after colony expansion re-initiated (Fig. 4a; yellow arrows). For the biofilm reporters P_{epsA}-*lux* and P_{tapA}-*lux*, expression was greatest at the growing edge during colony expansion (Fig. 4a; blue arrows) and for a short duration at the ring edge after expansion paused, decreasing when colony expansion re-initiated (Fig. 4a; yellow arrows). For P_{spoIIG}-*lux* and P_{spoIID}-*lux*, most expression occurred after colony expansion paused but decreased when colony expansion re-initiated (Fig. 4a; yellow arrows). Greatest P_{spoIIG}-*lux* and P_{spoIID}-*lux* expression occurred about a day after greatest P_{epsA}-*lux* and P_{tapA}-*lux* expression, suggesting a temporal organization whereby

matrix forms before sporulation is activated. There was re-activation of the P_{epsA}-*lux*, P_{spoIIG}-*lux and* P_{spoIID}-*lux* in rings 1 and 2 48 h after the initial bioluminescence pulse (Fig. 4a, yellow arrows). Inspection of kymographs also highlighted similar but less pronounced patterns for P_{ytvA}-*lux* and P_{tapA}-*lux* (Fig. 4a). Periodicities that are harmonics or multiples of a 24 h cycle occur elsewhere, such as in specific mammalian cell lines and insects[37,38].

Internal synchrony

A key feature of circadian organisation is internal synchrony. For instance, humans show a striking change in the internal circadian clock-regulated phase relationships when moving from entrained to free-running conditions[39], a demonstration of oscillator theory in the active interaction of circadian clocks with external and internal zeitgebers. The internal phase relationships between clock-regulated promoter-luciferase reporter activity and colony expansion rate were examined. In DD, the phases of the rhythms in the rate of colony expansion and bioluminescence (gene) expression from all reporters tested apart from P_{spoIID}-*lux* drifted apart as the colony developed (Fig. 4b; Supplementary Fig. 14a). In T24 bLD, two of four tested reporters re-positioned internal phase relationships, with expansion rate and reporter gene expression moving alternatively to antiphase (*epsA, spoIIG*) or to a similar phase (*ytvA*; Fig. 4c; Supplementary Fig. 14b). This suggests that the *B. subtilis* circadian clock regulates internal temporal synchrony of complex and diverse outputs, as observed in complex eukaryotes.

Discussion

We have identified that the circadian clock in *B. subtilis* is a hierarchical organizer of colony expansion and development. Using promoter-luciferase reporters and multi-day bioluminescence imaging of colonies formed on soft agar, we find novel and diverse clock-regulated processes in this prokaryote. Specifically, these pertain to colony expansion, transcription, and differentiation/development.

We found that biofilm matrix production reporters were robustly rhythmic in both pellicle biofilm-forming cultures and in expanding colonies on soft agar that lacked overt biofilm morphology. These reporters had greater expression in more opaque regions at the edge of colony rings, with both the opaque and translucent ring regions accumulating similar cell numbers. However, the opaque regions had greater peroxide resistance, which is characteristic of the presence of biofilm and spores. Given the absence of any obvious triggers for biofilm formation, it appears that the clock is capable of regulating this process in certain environments. A similar logic applies to sporulation, which is primarily driven by nutrient depletion or other stressful environmental conditions.

The phenotype we identified does not require electrochemical signalling through the action of the potassium channel YugO, whereas this is necessary for ultradian metabolic oscillations and colony patterning[9,32,40] (Supplementary Fig. 8). It is common that circadian and non-circadian oscillations exist in the same tissues. For example, the neurophysiology of the sleeping brain cycles through various frequencies, yet cells concurrently show a circadian rhythm[41]. In the cyanobacterium *Synechococcus elongatus* PCC 7942, the circadian clock leads to amplitude modulation of pulses of expression of RpoD4 that occur during cell division[42], opening an intriguing possibility that ultradian developmental processes in *B. subtilis*[9,43] could also be modulated by the circadian clock.

Regulation by the circadian clock can be understood with the heuristic of a simplified input-oscillator-output architecture that is thought to exist at all scales of operation[44,45]. Our findings here mainly concern new and diverse output pathways, with the circadian clock organizing specific internal phase relationships (time of day) and expression patterns for each promoter investigated. This organization is important: in mammals, internal synchrony affects health outcomes[46–49], and in plants, circadian coordination between tissues contributes to growth and reproduction[50,51]. Using *B. subtilis*, the regulation of known pathways can help to interpret the choreography of clock-regulated output pathways. For instance, SigB is regulated by diverse stress pathways, and in turn influences sporulation, biofilm formation, and competence[52–54]. The key molecular switch between activation of sporulation gene expression or lack thereof is phosphorylation and dephosphorylation. One mechanism by which SigB acts is through Spo0E, a phosphatase that inhibits the initiator of sporulation Spo0A[55]. Although this could form a mechanism by which the light/dark cycle acts through SigB to attenuate active Spo0A levels in the cells, *spoIIG* promoter activity is not acutely downregulated during the light phase of blue light/dark cycles under the conditions used in our experiments (Supplementary Fig. 12). Moreover, a Δ*sigB* knockout forms concentric growth rings (Fig. S15a), and retains circadian rhythmicity of P_{epsA}-*lux* and colony expansion rate during the colony spreading assay (Supplementary Fig. 15b, c), further suggesting that these clock-regulated pathways might not operate via SigB.

Internal synchrony is the key to circadian organization and has not been studied previously in microorganisms (e.g., fungi and cyanobacteria). It is a difficult concept to study due to the inherent complexity of circadian systems and the experimental tools available to perform time-series analyses. Our experiments allowed the spatial mapping of internal phase relationships within the colony over space and time, demonstrating that *B. subtilis* colonies show features of circadian organization. Control by the circadian clock produces specific spatiotemporal relationships between distinct developmental regulators during colony expansion, despite the apparent coupling of all these promoters to the clock. This suggests that the *B. subtilis* clock differentially regulates multiple developmental output pathways, and/or that circadian timing information is combined with other environmental information (e.g., nutrition or within-colony communication) to produce responses appropriate for each location within the colony. Given that there was less phase coherence between replicates for some reporters (Supplementary Fig. 16) and oscillations can occur spontaneously from the start of each experiment, it is possible that factors additional to light and temperature could act to entrain the clock in expanding colonies.

B. subtilis practices circadian organization reminiscent of circadian systems in multicellular eukaryotes, demonstrating that higher-order features of circadian clocks span across the kingdoms of life, including organisms where clocks likely have different molecular components. Importantly, our data provide a unique demonstration of internal (de- or re-) synchronization, which is a key aspect of circadian organization. In some experiments, we found that the phase relation between two clock-controlled processes changed during the experiment (Fig. 4b, c), which is reminiscent of the altering phase relationships between body temperature and sleep in humans under free-running conditions[56].

What is the benefit of circadian organization for *B. subtilis*? Biofilm formation is the predominant lifestyle of bacteria in nature and is an important driver of biogeochemical cycles[57], as well as providing resistance to ecologically and medically relevant environmental challenges such as antibiotics and ultraviolet radiation[58,59]. Similarly, spore formation is an essential fitness attribute, allowing bacteria to persist despite stresses such as low pH, dehydration, cold or nutrient deprivation[60–62]. Within its role during rhythmic colony expansion, the circadian clock might facilitate periodic cycles of foraging and feeding (colony expansion), followed by behaviours ensuring persistence and reproduction (colony pausing, preparation for biofilm deposition and sporulation). While matrix deposition occurs during, and is required for, colony expansion[28,63,64], reporter expression profiles suggest that it is accompanied by sporulation during periods of decreased growth. This could represent an adaptation to predictable fluctuations in the availability of nutrients in the environment, due to abiotic factors such

as soil nutrient mobilization, biotic factors such as cross-feeding, as well as daily rhythms in adverse environmental conditions such as antimicrobial production by other microorganisms or UV exposure. Given that this involves circadian coordination within the colony, it appears to represent a form of multicellular organization of circadian behaviour in *B. subtilis*. Multicellular organisation in bacteria is complex and important for ecology and pathology, with this study identifying a set of outputs of the *B. subtilis* circadian clock. We demonstrate that circadian regulation is deeply integrated into the growth and development of *B. subtilis*.

Methods

Strains and general culture conditions

Unless otherwise stated, *B. subtilis* was routinely grown in low salt lysogeny broth (LB, 10 g L^{-1} tryptone (Gibco), 5 g L^{-1} yeast extract (Gibco), 5 g L^{-1} NaCl (Sigma)), or on LB agar plates (2% (w/v) agar, Difco). The strains and vectors used in this study are reported in Supplementary Table 1.

Strain construction

The *B. subtilis* strains used were constructed by natural competence transformation using genomic or plasmid DNA. Overnight cultures of recipient strains were diluted at a 1:50 ratio with either competence medium (14.036 g L^{-1} K2HPO4·3H_2O, 5.239 g L^{-1} KH_2PO_4, 20 g L^{-1} glucose, 0.8823 g L^{-1} Na_3-citrate, 0.22 g L^{-1} ferric NH_4 citrate, 1 g L^{-1} casein hydrolysate, 2 g L^{-1} K-glutamate, 0.82 g L^{-1} $MgSO_4$·7H_2O, and 0.005 (w/v) % tryptophan) or glucose-casein hydrolysate-potassium phosphate buffer (GCHE) medium and incubated for 4 hours at 37 °C. Following the incubation period, 5 to 10 µg of genomic or plasmid DNA were added with 400 µl of competent cells and further incubated for 2 hours before plating on LB (Lennox, Carl Roth, 10 g l^{-1} tryptone, 5 g l^{-1} yeast extract and 5 g l^{-1} NaCl) agar supplemented with selective antibiotics. Successful transformation was validated using the reporter activity of the strains and PCR amplification of the mutant locus.

Agar media preparation, inoculation and incubation for ring formation assay

B. subtilis was inoculated in LB medium and cultured overnight. Cultures were then diluted to an optical density at 600 nm (OD_{600}) of 0.1 and grown until they reached an OD_{600} of 0.5. 2 µl of bacteria from this culture were spotted onto LB medium (recipe as above) with 0.55% (w/v) Difco agar at pH 6.0 (LB-agar). Square Petri dishes 120 × 120 × 17 mm (Greiner Bio-One) or circular Petri dishes (150 × 20 mm, Sarstedt) contained 75 ml or 60 ml of LB-agar medium, respectively. When standard-sized circular Petri dishes were used (92 × 16 mm, Sarstedt), they contained 25 ml of LB agar medium. Plates were always prepared the day before experiments, using freshly autoclaved media. Agar media was poured in a temperature-controlled room at 19 °C, and left open to dry for 10 minutes immediately after pouring. Plates were then kept closed overnight at 19 °C before use. Inoculated plates were sealed using parafilm, placed in incubators at a constant temperature of 27 °C and either incubated in constant darkness or subjected to different light or temperature cycles, as indicated in the text and figure legends. Samples were exposed to light using blue or red LEDs with peak emission at, respectively, 450 or 463 nm, or 625 nm (blue or red, respectively; Barthelme, Nürnberg, Germany). The average photon flux density was 30 µmol m^{-2} s^{-1}. Light intensity was measured using a spectroradiometer (Model IL1400A, International Light Inc., Newburyport, MA, USA or LI-COR LI-180, USA). Samples that were subjected to temperature cycles were kept on top of an LED plate emitting dim red light (13 µmol m^{-2} s^{-1}) in an otherwise dark incubator. All experiments were conducted in temperature-controlled incubators (Panasonic MIR-154 or MIR-553) with programmable temperature cycles.

At the end of the experiments, pictures were acquired using the Chemi-imager (ChemiDoc MP Imaging System, Bio-Rad) and Image Lab software (Version 5.1, Bio-Rad Laboratories). Colony areas were calculated using the image processing software Fiji[65].

Time-lapse infrared imaging of colony expansion

Square Petri dishes (120×120×17 mm, Greiner Bio-One) with 75 ml of 0.55% (w/v) LB-agar pH 6 were inoculated with *B. subtilis* 168 as described above. Plates were incubated in a dark, temperature-controlled incubator (Panasonic MIR-553) and placed upside-down on a red LED panel (13 µmol m^{-2} s^{-1}) to improve contrast during imaging. Time-lapse images were acquired every hour using an infrared camera (PH770 wildlife camera, Crenova) placed on top of the plate.

Luciferase imaging of expanding colonies

For colony bioluminescence imaging, *B. subtilis* 168 Jena was grown overnight (16-18 h) at 30 °C in an orbital shaker (120 rpm). Cells were reinoculated into LB at an OD_{600} of 0.05 and grown at 37 °C (120 rpm) until mid-exponential phase (OD_{600} ~ 0.4-0.6). 2 µL of bacteria was then spotted onto LB agar (0.55% (w/v), pH 6.0) in 14 cm diameter petri dishes. Once inoculated, plates were incubated for 120 h at 27 °C. Blue light was used for illumination where required, at a fluence rate of 30 µmol m^{-2} s^{-1}. In cases where colony growth stopped before the end of the experiment or colony shapes arose that could not be reliably analysed, these data were excluded (see Supplementary Data 2).

Retiga LUMO CCD cameras (Teledyne Photometrics) within temperature-controlled PHCBio MIR-554-PE incubators were used for bioluminescence imaging. Illumination was provided using custom-built LED panels, operated by an Arduino-controlled relay switch. LUMO cameras and LEDs were controlled using MicroManager v1.4.23 (https://micro-manager.org/) and custom BeanShell scripts[66] (http://beanshell.org/home.html) in association with ImageJ (Supplementary Software 1). Exposure times varied according to the reporter (60 s: P_{ytvA}-*lux*, P_{epsA}-*lux*, P_{tapA}-*lux*, P_{spoIIG}-*lux*; 1200 s: P_{spoIID}-*lux*). In colony expansion assays, the signal from P_{spoIIQ}-*lux* was too low for analysis even at 1200 s exposure. In constant darkness, bioluminescence images were obtained every 30 minutes for reporters requiring a 60 s exposure, and every hour for P_{spoIID}-*lux* where a longer exposure was required. In experiments in which samples were illuminated, LEDs were turned off for two minutes prior to, and during, exposure. Images were taken every hour under illuminated conditions to minimise interference with the lighting regime.

Growth curves of strains in liquid LB medium

To assess the effect of light on growth in liquid culture, overnight cultures were diluted to OD 0.1 in LB medium, and split equally into cultures that were incubated for 8 h under DD, constant blue or constant red light (both 30 µmol m^{-2} s^{-1}) under agitation (120 rpm) and constant temperature of 27 °C. OD_{600nm} was measured using a spectrometer (Ultrospec 3100 pro, Amersham Biosciences) at the indicated time points.

Luciferase luminometry in microplate culture

B. subtilis was grown overnight in LB medium, and the day after diluted to OD_{600} of 0.05, and grown in nutrient sporulation medium (NSMP; nutrient broth (8 g l^{-1}) (Difco), 1 µmol l^{-1} $FeCl_3$, 700 µmol l^{-1} $CaCl_2$, 50 µmol l^{-1} $MnCl_2$, 1 mmol l^{-1} $MgCl_2$, and 100 mM potassium phosphate)[67]. The media was supplemented with 0.05% (w/v) glucose. Liquid cultures for measuring bioluminescence were grown in white 96-well plates (Nunclon Delta, Thermo Fisher Scientific), with each well inoculated with 5 × 10^5 cells. Plates were sealed with a transparent evaporation-free cover (Optical Adhesive Covers, Applied Biosystems, Life Technologies). Bioluminescence was measured (Berthold Centro LB960 XS3 or Berthold Mithras LB 940 Multimode Plate Reader) for 1 s each hour. All experiments occurred in temperature-controlled

incubators (either MIR-154, Panasonic, Japan, or Percival Intellus, Percival, USA). For experiments involving entrainment using light, the microplate was ejected from the machine between readings for exposure to light. Within the data, each sample was one well of the microreader plate.

Strain 168 expressing the sporulation reporters P_{spoIIG}-*lux*, P_{spoIIQ}-*lux*, P_{spoIID}-*lux*, the biofilm reporters P_{epsA}-*lux* or P_{tapA}-*lux*, or the control reporter P_{ytvA}-*lux* were incubated for 5 days under 24 h bLD cycles (12 h dark/12 h blue light, 30 µmol m^{-2} s^{-1}), followed by release to constant darkness for 3 days. The temperature was 27 °C during the entire experiment.

Microscopic quantification of total cell number across the colony

Soft agar plates were inoculated with 168 constitutively expressing the fluorescent protein mKate2 ($P_{hyperspank}$-*mKate2*) to monitor cell number. Plates were incubated in darkness at 27 °C for 4 days. Biopsies were taken from both translucent and opaque sections of the rings and inverted onto a glass-bottomed microscope plate. The agar covering the top layer of cells was removed to improve clarity during microscopy. mKATE2 images were acquired using an inverted microscope (Ti2-E, Nikon) equipped with a camera for fluorescence detection (DS-Qi2 camera, Nikon). For signal quantification, images were processed using the NIS-Elements software (Nikon). Background signal was removed using background ROIs, and detection and segmentation of single cells allowed calculation from the mKATE2 of a read-out for total cell number in different sections of the rings.

CFU determination

Bacteria were grown on soft agar plates in DD for 4 days at 27 °C. Bacteria were excised from the opaque and translucent portions of 1-, 2- or 3-day-old rings, as indicated in Fig S3, using a Pasteur pipette. The content of each biopsy was resuspended in 1 ml of PBS. To count cell number, cells were first sonicated for two or three cycles of 30 s each (Bioruptor Plus, Diagenode) to disrupt cells without loss of viability. Following serial dilutions, sonicated cells were plated on LB agar and grown overnight at 37 °C. The number of colony-forming units (CFUs) was counted the following day.

Hydrogen peroxide-sensitivity assay

Bacteria were grown on soft agar plates under DD for 4 days, at 27 °C. Bacteria were excised from the opaque and translucent portions of 2- or 3-day-old rings as indicated, using a Pasteur pipette. An aliquot was removed to count cell number, and the remainder was subjected to peroxide stress. To measure peroxide stress resistance, bacteria were exposed to 60 mM H_2O_2 for 90 minutes, followed by serial dilutions, plating, and CFU-counting the next day. For each sample, the percentage of survival was calculated as the ratio between the CFUs after peroxide exposure and the CFUs from corresponding sonicated biofilms that were not peroxide-treated.

Analysis of time-lapse imaging of colony area

Time-lapse image processing to determine colony area was conducted using a customized ImageJ/Fiji macro[65] (Supplementary Software 2). Briefly, all frames were included in a stack where each frame was set to have the same brightness and contrast. The signal was then inverted to create a bright signal over a dark background. Background noise was removed using the region of interest (ROI) manager. The image was cropped to include only the area of interest for analysis, converted to binary, and thresholded so that in each frame only the colony was selected. Since the colony expanded with time, this allowed the software to detect and select the colony size at the different time points. The thresholded area in each frame was calculated. Finally, the area of the colony mask was measured for each frame (time point) within the stack, yielding a time series of colony area values.

Analysis of luciferase luminometry in microplate culture

For the analysis of the luciferase luminometry in microplate culture (Fig. 3b), samples were first subjected to the (Classic) JTK test for rhythmicity with a statistical cut-off of $p < 0.05$. The p-values were corrected by the Benjamini–Hochberg procedure for multiple testing. The FRP of the rhythmic samples was calculated for three days following two hours after release in constant darkness using the maximum entropy spectral analysis (MESA) method in BioDare2 following baseline detrending. The proportion of samples exhibiting circadian rhythmicity is shown in Supplementary Fig. 9b.

Analysis of time-series bioluminescence imaging data from expanding colonies

Image processing and data extraction were performed using Fiji (Fiji Macros S1-S7[65]; https://imagej.net/software/fiji/) version 1.53c. Intensity histogram limits were adjusted across the entire images to optimize contrast, ensuring no clipping of high or low signal. Several ImageJ macros were developed for the semi-automated extraction of various types of data from the bioluminescence time-series. Individual colonies were cropped from time series images that included several separate plates and saved as individual image stacks. Intensity thresholding (Supplementary Data 2) was then applied to delimit the colony from the background agar, and masks of the entire colony were created. Using the resulting masks, bioluminescence intensity data (as mean grey value) and colony area were extracted from the entire time series. To obtain data on the bioluminescence intensity at the growing colony edge, these masks were converted to outlines, the region 4 pixels either side of the colony outline was selected, and further masks were created for the region spanning 4 pixels either side of the outline. Combining these masks with those of the whole colony allowed the selection of the region 4 pixels within the edge of the colony. Mean bioluminescence intensity data were then extracted from this region throughout the image stack. The Fiji Macros for these purposes can be found in Supplementary Software 2 (Fiji Macros S1-S5[66]).

Rhythmicity, period, and phase analyses of whole colony and edge bioluminescence, and colony expansion rate were performed using BioDare2[68] (https://biodare2.ed.ac.uk/). Samples were first screened for rhythmicity, using the BD2 eJTK method (BD2 Classic analysis preset), which is suited to rhythms having periods that can be outside of the 22–26 h range[69]. Benjamini-Hochberg p-value correction was used with $p < 0.05$ for rhythm detection. Period was estimated from rhythmic samples using the fast Fourier transform – non-linear least squares (FFT-NLLS) method. Samples were screened by their fit to the data and filtered using a relative amplitude error (RAE) cut-off of 0.6. Manual inspection was used to distinguish between multiple potential model fits satisfying these criteria. Phase data were extracted for experiments performed under T24 bLD as the average phase of all the peaks within the analyzed time window expressed relative to the first exposure to blue light (12 h post-inoculation). These analyses were performed on data within the window of 12–84 h post-inoculation.

Generation of kymographs

To produce kymographs, the centre point of each colony was located and each image in the time-series polar transformed around this point to linearize the image, using 360° of polar space, through batch processing with the Polar Transformer plugin for Fiji (https://imagej.net/ij/plugins/polar-transformer.html). Each degree of polar space corresponds to a radial slice of the colony image represented as a single pixel-wide slice in the polar-transformed image. Using a custom Fiji macro (Supplementary Software 2), the intensity profile for each linearized radial slice was obtained for all images in the time series, producing one intensity profile along each radial slice for each time point. The profiles generated for each radial slice were stacked on top of one another to create each kymograph. This created a total of 360 kymographs, each corresponding to one radial slice in polar space.

Average intensity projections were then made using this image stack to examine dynamics around the full 360° of polar space.

Analysis of internal phase relationships

For examination of internal phase relationships between colony expansion rate and edge bioluminescence rhythms, peak times were extracted by fitting cubic splines to raw data using the smooth.spline R package[70] (for smoothing parameters and number of knots used see Supplementary Data 2) and the second-order derivative calculated at each time-point in the time-series using the predict package[70]. This allowed the identification of inflection points in the data through the identification of a change in the sign of the second derivative. Inflection points identifying a change from a positive to a negative first-order derivative were then filtered manually for those corresponding to major peaks in the data.

For data collected in constant darkness, the first bioluminescence peaks identified were used to align both the edge bioluminescence and colony expansion rate data from all analyzed colonies (Supplementary Fig. 16), setting the time of the first bioluminescence peak to 0. Subsequent peak times were then expressed relative to this time on a scale of 0–24 h for each subsequent 24 h period, and normalized to the period of the colony expansion rhythm using Eq. 1.

$$t_norm = t \cdot (24/\tau ER) \quad (1)$$

Where t is peak time, and t_{norm} is the normalized peak time, and τ_{ER} is the expansion rate period. For experiments performed under T24 bLD, peak time was expressed relative to dawn (ZT0, 12 h post-inoculation), with no normalization to the period of either rhythm.

For presentation, data were routinely detrended using a 3rd degree polynomial fitting method within the DetrendTimeSeries function (FCSlib package)[71], and normalized by calculating a Z-score, where x is the bioluminescence signal (Eq. 2).

$$Z = (x - \mathrm{mean}(x))/(\mathrm{sd}(x)) \quad (2)$$

All graphs were generated with ggplot2. Double-plot actograms were produced using the Rethomics R packages behavr, damr and ggetho[72]. Detrended and Z-score normalized data were transformed by removing all negative values and this data was then used to plot actograms using the ggetho package.

Statistical analysis and data visualization

Statistical analysis was performed either using R (version 4.3.3, 2024-02-29) or GraphPad Prism 8 (version 8.4.3). For analyses using R, data were tested for normality using a Shapiro-Wilk test, and equality of variance between samples was verified using a Bartlett's test (e.g., for Figs. 3b, g and S3; variances were sometimes unequal). Where appropriate, general (normally distributed data with equal variance between sample groups; Fig. 3g, Supplementary Figs. 1c, 3) or generalized linear models (non-normal data or unequal sample variances; Fig. 3b, Supplementary Fig. 10f) were built, including all possible higher order interactions, and model reduction performed subsequently with likelihood ratio testing, removing the highest order non-significant interactions first. Minimal models were used for statistical analysis and ANOVA or ANODE (Analysis of Deviance) tables were produced for formal analysis from general or generalized linear models, respectively. Post-hoc multiple comparisons following linear modelling were made using the emmeans package[73]. Two-tailed t-tests or two-sample Wilcoxon tests (Mann-Whitney tests) were performed using appropriate R packages. Linear regression was performed by fitting linear models to the data and Pearson's correlation coefficients (PCC's) were generated using the R package Cor (Fig. 3h, Supplementary Fig. 11). To calculate the colony expansion rate, cubic splines were fitted to raw colony area data using the smooth.spline R package (smoothing parameter = 0.5) and the first-order derivative calculated at each time-point in the time-series using the Predict package[70]. For analysis of bacterial growth curves (e.g., Supplementary Fig. 1c), cubic splines were fitted to raw colony area data (using generalised cross-validation for smoothing parameter computation) and the first-order derivative calculated at each time-point in the time-series using the Predict package. From these values, the maximum was selected as the maximal growth rate (r_0) and the time at which this rate was reached was extracted. For Fig. 3i (H_2O_2 treatment), the Mann-Whitney test was used, assessed as the ratio of CFU after peroxide exposure to CFU prior H_2O_2 exposure, from sonicated biopsies of colonies.

Reporting summary

Further information on research design is available in the Nature Portfolio Reporting Summary linked to this article.

Data availability

All source data are provided as a Source Data file. Source data are provided with this paper.

Code availability

Data analysis code is provided in Supplementary Software 1 (Beanshell scripts) and Supplementary Software 2 (Fiji macros), with this code deposited at Zenodo (https://doi.org/10.5281/zenodo.19821962).

References

1. Merrow, M., Spoelstra, K. & Roenneberg, T. The circadian cycle: daily rhythms from behaviour to genes. *EMBO Rep.* **6**, 930–935 (2005).
2. Panda, S. Circadian physiology of metabolism. *Science (1979)* **354**, 1008–1015 (2016).
3. Jabbur, M. L., Dani, C., Spoelstra, K., Dodd, A. N. & Johnson, C. H. Evaluating the Adaptive Fitness of Circadian Clocks and their Evolution. *J. Biol. Rhythms* **39**, 115–134 (2024).
4. Golden, S. S. & Canales, S. R. Cyanobacterial circadian clocks - Timing is everything. *Nat. Rev. Microbiol.* **1**, 191–199 (2003).
5. Paulose, J. K., Wright, J. M., Patel, A. G. & Cassone, V. M. Human Gut Bacteria Are Sensitive to Melatonin and Express Endogenous Circadian Rhythmicity. *PLoS One* **11**, e0146643 (2016).
6. Eelderink-Chen, Z. et al. A circadian clock in a nonphotosynthetic prokaryote. *Sci. Adv.* **7**, eabe2086 (2021).
7. Arnaouteli, S., Bamford, N. C., Stanley-Wall, N. R. & Kovács, Á T. *Bacillus subtilis* biofilm formation and social interactions. *Nat. Rev. Microbiol.* **19**, 600–614 (2021).
8. Jeckel, H. et al. Simultaneous spatiotemporal transcriptomics and microscopy of *Bacillus subtilis* swarm development reveal cooperation across generations. *Nat. Microbiol.* **8**, 2378–2391 (2023).
9. Chou, K. et al. A segmentation clock patterns cellular differentiation in a bacterial biofilm. *Cell* **185**, 145–157 (2022).
10. Dergham, Y. et al. Direct comparison of spatial transcriptional heterogeneity across diverse *Bacillus subtilis* biofilm communities. *Nat. Commun.* **14**, 7546 (2023).
11. Otto, S. B. et al. Privatization of biofilm matrix in structurally heterogeneous biofilms. *mSystems* **5**, 525 (2020).
12. Sartor, F., Kovács, Á & T Rhythmic spatial self-organization of bacterial colonies. *mBio* **13**, e0170322 (2022).
13. Harmer, S. L. et al. Orchestrated Transcription of Key Pathways in *Arabidopsis* by the Circadian Clock. *Science (1979)* **290**, 2110–2113 (2000).
14. Panda, S. et al. Coordinated transcription of key pathways in the mouse by the circadian clock. *Cell* **109**, 307–320 (2002).

15. Roenneberg, T. & Foster, R. G. Twilight times: light and the Circadian system. *Photochem. Photobiol.* **66**, 549–561 (1997).
16. Sartor, F. et al. The circadian clock of the bacterium *B. subtilis* evokes properties of complex, multicellular circadian systems. *Sci. Adv.* **9**, eadh1308 (2023).
17. Aschoff, J. & Pohl, H. Phase relations between a circadian rhythm and its zeitgeber within the range of entrainment. *Naturwissenschaften* **65**, 80–84 (1978).
18. Bruce, V. Environmental entrainment of circadian rhythms. in *Cold Spring Harbor Symp. Quant. Biol.* **25**, 29–48 (1960).
19. Merrow, M., Brunner, M. & Roenneberg, T. Assignment of circadian function for the *Neurospora* clock gene frequency. *Nature* **399**, 584–586 (1999).
20. Calvio, C. et al. Swarming differentiation and swimming motility in *Bacillus subtilis* are controlled by *swrA*, a newly identified dicistronic operon. *J. Bacteriol.* **187**, 5356–5366 (2005).
21. Senesi, S. et al. Surface-associated flagellum formation and swarming differentiation in *Bacillus subtilis* are controlled by the *ifm* locus. *J. Bacteriol.* **186**, 1158–1164 (2004).
22. Ghelardi, E. et al. Contribution of surfactin and SwrA to flagellin expression, swimming, and surface motility in *Bacillus subtilis*. *Appl. Environ. Microbiol.* **78**, 6540–6544 (2012).
23. Stevens, A. & Søgaard-Andersen, L. Making waves: pattern formation by a cell-surface-associated signal. *Trends Microbiol* **13**, 249–252 (2005).
24. Reid, C. R. & Latty, T. Collective behaviour and swarm intelligence in slime moulds. *FEMS Microbiol. Rev.* **40**, 798–806 (2016).
25. Patrick, J. E. & Kearns, D. B. Laboratory strains of *Bacillus subtilis* do not exhibit swarming motility. *J. Bacteriol.* **191**, 7129–7133 (2009).
26. Kearns, D. B., Chu, F., Rudner, R. & Losick, R. Genes governing swarming in *Bacillus subtilis* and evidence for a phase variation mechanism controlling surface motility. *Mol. Microbiol.* **52**, 357–369 (2004).
27. Hölscher, T. & Kovács, Á. T. Sliding on the surface: bacterial spreading without an active motor. *Environ. Microbiol.* **19**, 2537–2545 (2017).
28. Grau, R. R. et al. A duo of potassium-responsive Histidine Kinases govern the multicellular destiny of *Bacillus subtilis*. *mBio* **6**, e00581 (2015).
29. van Gestel, J., Weissing, F. J., Kuipers, O. P. & Kovács, ÁT. Density of founder cells affects spatial pattern formation and cooperation in *Bacillus subtilis* biofilms. *ISME J.* **8**, 2069–2079 (2014).
30. Tiensuu, T., Andersson, C., Rydén, P. & Johansson, J. Cycles of light and dark co-ordinate reversible colony differentiation in *Listeria monocytogenes*. *Mol. Microbiol.* **87**, 909–924 (2013).
31. Kahl, L. J., Eckartt, K. N., Morales, D. K., Price-Whelan, A. & Dietrich, L. E. P. Light/dark and temperature cycling modulate metabolic electron flow in *Pseudomonasaeruginosa* Biofilms. *mBio* **13**, e0140722 (2022).
32. Yang, C.-Y. et al. Encoding membrane-potential-based memory within a microbial community. *Cell Syst.* **10**, 417–423.e3 (2020).
33. Muratov, E., Keilholz, J., Kovács, Á. & Moeller, R. The biofilm matrix protects *Bacillus subtilis* against hydrogen peroxide. *Biofilm* **9**, 100274 (2025).
34. Welsh, D. K., Logothetis, D. E., Meister, M. & Reppert, S. M. Individual neurons dissociated from rat suprachiasmatic nucleus express independently phased circadian firing rhythms. *Neuron* **14**, 697–706 (1995).
35. Harrington, M. et al. Behavioral and neurochemical sources of variability of circadian period and phase: studies of circadian rhythms of npy-/- mice. *Am. J. Physiol. Regul. Integr. Comp. Physiol.* **292**, R1306–R1314 (2007).
36. Zhang, R., Lahens, N. F., Ballance, H. I., Hughes, M. E. & Hogenesch, J. B. A circadian gene expression atlas in mammals: implications for biology and medicine. *Proc. Natl. Acad. Sci. USA.* **111**, 16219–16224 (2014).
37. Wang, Y. et al. Circabidian rhythm of sex pheromone reception in a scarab beetle. *Curr. Biol.* **34**, 568–578.e5 (2024).
38. Hughes, M. E. et al. Harmonics of circadian gene transcription in mammals. *PLoS Genet.* **5**, e1000442 (2009).
39. Aschoff, J. & Wever, R. Human circadian rhythms: a multioscillatory system. *Fed. Proc.* **35**, 236–32 (1976).
40. Prindle, A. et al. Ion channels enable electrical communication in bacterial communities. *Nature* **527**, 59–63 (2015).
41. Scammell, T. E., Arrigoni, E. & Lipton, J. O. Neural circuitry of wakefulness and sleep. *Neuron* **93**, 747–765 (2017).
42. Ye, C. et al. The cyanobacterial circadian clock couples to pulsatile processes using pulse amplitude modulation. *Curr. Biol.* **34**, 5796–5803.e6 (2024).
43. Liu, J. et al. Metabolic co-dependence gives rise to collective oscillations within biofilms. *Nature* **523**, 550–554 (2015).
44. Eskin, A. Identification and physiology of circadian pacemakers. *Introduction. Fed. Proc.* **38**, 2570–2605 (1979).
45. Pittendrigh, C. S. & Bruce, V. G. V. An Oscillator Model for Biological Clocks. In *Rhythmic and Synthetic Processes in Growth* 75–110. Princeton University Press. https://doi.org/10.1515/9781400876167-006. (1958).
46. Willett, W. C. et al. Rotating night shifts and risk of breast cancer in women participating in the nurses' health study. *J. Natl. Cancer Inst.* **93**, 1563–1568 (2001).
47. Schernhammer, E. S. et al. Night-shift work and risk of colorectal cancer in the nurses' health study. *JNCI J. Natl. Cancer Inst.* **95**, 825–828 (2003).
48. Scheer, F. A. J. L., Hilton, M. F., Mantzoros, C. S. & Shea, S. A. Adverse metabolic and cardiovascular consequences of circadian misalignment. *Proc. Natl. Acad. Sci. USA.* **106**, 4453–4458 (2009).
49. Morris, C. J., Purvis, T. E., Hu, K. & Scheer, F. A. J. L. Circadian misalignment increases cardiovascular disease risk factors in humans. *Proc. Natl. Acad. Sci. USA.* **113**, E1402–E1411 (2016).
50. Sawa, M. & Kay, S. A. GIGANTEA directly activates *Flowering Locus T* in *Arabidopsis thaliana*. *Proc. Natl. Acad. Sci.* **108**, 11698–11703 (2011).
51. Chew, Y. H. et al. Multiscale digital *Arabidopsis* predicts individual organ and whole-organism growth. *Proc. Natl. Acad. Sci.* **111**, 4127–4136 (2014).
52. Bartolini, M. et al. Regulation of biofilm aging and dispersal in *Bacillus subtilis* by the alternative Sigma Factor SigB. *J. Bacteriol.* **201**, e00473–18 (2019).
53. Reder, A., Albrecht, D., Gerth, U. & Hecker, M. Cross-talk between the general stress response and sporulation initiation in *Bacillus subtilis* – the σ^B promoter of *spo0E* represents an AND-gate. *Environ. Microbiol.* **14**, 2741–2756 (2012).
54. Harms, M. et al. Activation of the general stress response sigma factor SigB prevents competence development in *Bacillus subtilis*. *mBio* **15**, e0227424 (2024).
55. Burbulys, D., Trach, K. A. & Hoch, J. A. Initiation of sporulation in *B. subtilis* is controlled by a multicomponent phosphorelay. *Cell* **64**, 545–552 (1991).
56. Aschoff, J., Gerecke, U. & Wever, R. Desynchronization of human circadian rhythms. *Jpn. J. Physiol.* **17**, 450–457 (1967).
57. Flemming, H.-C. & Wuertz, S. Bacteria and archaea on Earth and their abundance in biofilms. *Nat. Rev. Microbiol.* **17**, 247–260 (2019).
58. Flemming, H.-C. & Wingender, J. The biofilm matrix. *Nat. Rev. Microbiol.* **8**, 623–633 (2010).
59. Flemming, H. C. et al. Biofilms: An emergent form of bacterial life. *Nat. Rev. Microbiol.* **14**, 563–575 (2016).
60. Chubukov, V. & Sauer, U. Environmental dependence of stationary-phase metabolism in *Bacillus subtilis* and *Escherichia coli*. *Appl. Environ. Microbiol.* **80**, 2901–2909 (2014).

61. Illades-Aguiar, B. & Setlow, P. Autoprocessing of the protease that degrades small, acid-soluble proteins of spores of *Bacillus* species is triggered by low pH, dehydration, and dipicolinic acid. *J. Bacteriol.* **176**, 7032–7037 (1994).
62. Budde, I., Steil, L., Scharf, C., Völker, U. & Bremer, E. Adaptation of *Bacillus subtilis* to growth at low temperature: a combined transcriptomic and proteomic appraisal. *Microbiology* **152**, 831–853 (2006).
63. Gestel, J. V.aN. et al. Division of labor in biofilms: the ecology of cell differentiation. *Microbiol. Spectr.* **3**, 1–24 (2015).
64. Jautzus, T., van Gestel, J. & Kovács, ÁT. Complex extracellular biology drives surface competition during colony expansion in *Bacillus subtilis*. *ISME J.* **16**, 2320–2328 (2022).
65. Schindelin, J. et al. Fiji: an open-source platform for biological-image analysis. *Nat. Methods* **9**, 676–682 (2012).
66. Dorling, J. Supplementary code for Nature Communications manuscript NCOMMS-26-021071-T. Preprint at https://doi.org/10.5281/zenodo.19821962 (2026).
67. Fortnagel, P. & Freese, E. Analysis of sporulation mutants. II. Mutants blocked in the citric acid cycle. *J. Bacteriol.* **95**, 1431–1438 (1968).
68. Moore, A., Zielinski, T. & Millar, A. J. Online period estimation and determination of rhythmicity in circadian data, using the BioDare data infrastructure. *Methods Mol. Biol.* **1158**, 13–44 (2014).
69. Zieliński, T., Hay, J. & Millar, A. J. Period Estimation and Rhythm Detection in Timeseries Data Using BioDare2, the Free, Online, Community Resource. *Methods Mol. Biol.* **2398**, 15–32 (2022).
70. R Core Team. R: A Language and Environment for Statistical Computing. R Foundation for Statistical Computing, Vienna, Austria. https://www.R-project.org/ (2024).
71. Pinto-Cámara, R. et al. FCSlib: an open-source tool for fluorescence fluctuation spectroscopy analysis for mobility, number and molecular brightness in R. *Bioinformatics* **37**, 1930–1931 (2021).
72. Geissmann, Q., Garcia Rodriguez, L., Beckwith, E. J. & Gilestro, G. F. Rethomics: An R framework to analyse high-throughput behavioural data. *PLoS One* **14**, e0209331 (2019).
73. Searle, S. R., Speed, F. M. & Milliken, G. A. Population marginal means in the linear model: an alternative to least squares means. *Am. Stat.* **34**, 216–221 (1980).

Acknowledgements

We thank A. Bauer, T. Popp, and H. Klausner (University of Munich) for technical support.

Author contributions

Conceptualization: F.S. Experimental Design: F.S., A.N.D., J.D., M.M. Formal Analysis: F.S., J.D., B.F.B., E.G., Z.E.C., E.B. Funding acquisition: F.S., A.N.D., Á.T.K., M.M. Experimentation: F.S., J.D., E.G., Z.E.C., E.B., A.J., X.X., R.A., I.K.B. Visualization: J.D., F.S. Supervision: M.M., A.N.D., Á.T.K. Writing – original draft: F.S., J.D., Á.T.K., A.N.D., M.M. Writing – review & editing: all authors

Funding

Work in the AND lab is funded by UKRI-BBSRC (BB/X512229/1, BB/Z516636/1, Institute Strategic Programme BRiC BB/X01102X/1), the John Innes Centre, and the Chadacre Agricultural Trust (to IKB). Work in the MM lab is supported by the Volkswagen Foundation (Life Funding Program: "The Fourth Dimension"), the German Science Foundation (DFG Project 507872050), the Friedrich Bauer Stiftung (to FS) and the Verein zur Förderung von Wissenschaft und Forschung of the University of Munich (to FS). ÁTK and XX were supported by a Startup package from the Institute of Biology Leiden. The MM, AND and ÁTK laboratories are funded by the European Union (ERC, Synergy award 101166968 "MicroClock"). Views and opinions expressed are those of the author(s) only and do not necessarily reflect those of the European Union or the European Research Council Executive Agency. Neither the European Union nor the granting authority can be held responsible for them.

Competing interests

The authors declare no competing interests.

Additional information

Supplementary information The online version contains supplementary material available at https://doi.org/10.1038/s41467-026-74082-0.

Correspondence and requests for materials should be addressed to Antony N. Dodd or Martha Merrow.

Peer review information *Nature Communications* thanks Ilana Kolodkin-Gal and the other anonymous reviewers for their contribution to the peer review of this work. A peer review file is available.

Reprints and permissions information is available at http://www.nature.com/reprints

Publisher's note Springer Nature remains neutral with regard to jurisdictional claims in published maps and institutional affiliations.

Open Access This article is licensed under a Creative Commons Attribution-NonCommercial-NoDerivatives 4.0 International License, which permits any non-commercial use, sharing, distribution and reproduction in any medium or format, as long as you give appropriate credit to the original author(s) and the source, provide a link to the Creative Commons licence, and indicate if you modified the licensed material. You do not have permission under this licence to share adapted material derived from this article or parts of it. The images or other third party material in this article are included in the article's Creative Commons licence, unless indicated otherwise in a credit line to the material. If material is not included in the article's Creative Commons licence and your intended use is not permitted by statutory regulation or exceeds the permitted use, you will need to obtain permission directly from the copyright holder. To view a copy of this licence, visit http://creativecommons.org/licenses/by-nc-nd/4.0/.

© The Author(s) 2026